Unusual structure of the oxygen-binding site in the dimeric bacterial hemoglobin from *Vitreoscilla* sp.

Cataldo Tarricone[1,2], Alessandro Galizzi[1], Alessandro Coda[1], Paolo Ascenzi[3] and Martino Bolognesi[1,4]*

Background: The first hemoglobin identified in bacteria was isolated from *Vitreoscilla stercoraria* (VtHb) as a homodimeric species. The wild-type protein has been reported to display medium oxygen affinity and cooperative ligand-binding properties. Moreover, VtHb can support aerobic growth in *Escherichia coli* with impaired terminal oxidase function. This ability of VtHb to improve the growth properties of *E. coli* has important applications in fermentation technology, assisting the overexpression of recombinant proteins and antibiotics. Oxygen binding heme domains have been identified in chimeric proteins from bacteria and yeast, where they are covalently linked to FAD- and NAD(P)H-binding domains. We investigate here the fold, the distal heme site structure and the quaternary assembly of a bacterial hemoglobin which does not bear the typical flavohemoglobin domain organization.

Results: The VtHb three-dimensional structure conforms to the well known globin fold. Nevertheless, the polypeptide segment connecting helices C and E is disordered, and residues E7–E10 (defined according to the standard globin fold nomenclature) do not adopt the usual α-helical conformation, thus locating Gln53(E7) out of the heme pocket. Binding of azide to the heme iron introduces substantial structural perturbations in the heme distal site residues, particularly Tyr29(B10) and Pro54(E8). The quaternary assembly of homodimeric VtHb, not observed before within the globin family, is based on a molecular interface defined by helices F and H of both subunits, the two heme iron atoms being 34 Å apart.

Conclusions: The unusual heme distal site structure observed shows that previously undescribed molecular mechanisms of ligand stabilization are operative in VtHb. The polypeptide chain disorder observed in the CE region indicates a potential site of interaction with the FAD/NADH reductase partner, in analogy with observations in the chimeric flavohemoglobin from *Alcaligenes eutrophus*.

Addresses: [1]Dipartimento di Genetica e Microbiologia, Università di Pavia, Via Abbiategrasso 207, 27100 Pavia, Italy, [2]Dipartimento di Sciensa e Tecnologia del Farmaco, Università di Torino, Via P. Giuria 9, 10125 Torino, Italy, [3]Dipartimento di Biologia, Terza Università di Roma, Viale G. Marconi 446, 00146 Roma, Italy and [4]Centro Biotecnologie Avanzate - IST and Dipartimento di Fisica, Università di Genova, Largo R. Benzi 10, 16132 Genova, Italy.

*Corresponding author.
E-mail: bolog@ipvgen.unipv.it

Keywords: bacterial hemoglobin, nonvertebrate globin structure, oxygen-binding heme domains, *Vitreoscilla* sp. hemoglobin

Received: 27 January 1997
Revisions requested: 11 February 1997
Revisions received: 25 February 1997
Accepted: 25 February 1997

Electronic identifier: 0969-2126-005-00497

Structure 15 April 1997, 5:497–507

Introduction

Oxygen transport by hemoproteins is a widespread biological function which has been recognized in vertebrate and invertebrate phyla, in plants, fungi, protists and prokaryotes [1–4]. Similarities between the amino acid sequences and three-dimensional (3D) structures of hemoglobin (Hb) and myoglobin (Mb) outline a common evolutionary origin [5–8]. The molecular architecture of Hb and Mb is based on the well characterized globin fold, consisting of seven to eight α helices defining the heme pocket and the oxygen-binding site (for standard globin fold nomenclature see [9]). More than 700 amino acid sequences, together with more than two dozen crystal structures, from monomeric and oligomeric globins, characterize this homology family [6,10,11].

Two-domain oxygen-binding proteins, resulting from the fusion of an N-terminal heme-binding domain with a flavin-binding domain, have been identified in baceria and yeast. These proteins have tentatively been assigned functions related to cell signaling and regulation [12,13]. The crystal structure of *Alcaligenes eutrophus* bacterial flavohemoglobin (*Alcaligenes* flavoHb) [14] has shown that the N-terminal heme domain is closely related to the globin fold. On the other hand, the covalently connected FAD-dependent oxidoreductase module is structurally related to ferredoxin $NADP^+$ reductase [15], phtalate dioxygenase reductase [16], the FAD/NADH-binding fragment of nitrate reductase [17] and NADH cytochrome b_5 reductase [18], whose 3D structures are known. A different example of a heme containing chimeric protein is FixL, a *Rhizobium* signal transducing protein that regulates nitrogen fixation in response to oxygen levels. In FixL, an N-terminal oxygen sensor heme domain is fused to a C-terminal domain endowed with kinase activity [19].

In the strictly aerobic Gram-negative bacterium *Vitreoscilla*, oxygen-limited growth conditions (when atmospheric O_2 concentrations fall by more than 90%) can induce a 50-fold increase in the expression of a homodimeric hemoprotein

(146×2 amino acid residues) which was recognized as the first bacterial Hb [20]. This protein has been proposed to facilitate oxygen diffusion to the bacterial terminal oxidases, or to act itself as a terminal oxidase [2,21–23]. *Vitreoscilla* Hb (VtHb, previously known as cytochrome *o*) shows remarkable amino acid sequence identity (43–56%) with the heme domain of bacterial and yeast flavoHbs. However, much lower sequence identities (<20%) are observed with respect to Hb and Mb from plants and higher phyla. (One exception to this trend is leghemoglobin, which shares 26% amino acid identity with VtHb.) Nevertheless, VtHb contains two invariant residues found in other globins (PheCD1 and HisF8) and achieves significant scoring in comparisons with the globin sequence templates of Bashford *et al.* [11] and Moens *et al.* [8], indicative of essential conservation of the globin fold even in this bacterial Hb. In this framework, the role of the distal E7 residue has been assigned to Gln53 [2,20]. The reported O_2 affinity of VtHb (P_{50} = 16.7 mm Hg) is comparable to that of cyanide and carbon monoxide, whose binding to VtHb has been shown to be cooperative. Moreover, reduction of the ferric protein follows biphasic kinetics, the two hemes showing different redox potentials [2,24–27].

VtHb has been cloned and expressed in *Escherichia coli*, where it is located in the cytoplasm and can also be found in the periplasmic space [28]. Heterologous expression of VtHb results in a significant improvement of the growth properties of *E. coli* under low oxygen tension, through an increase in the level and activity of the bacterial terminal oxidases [21,22,28]. Such properties have found applications in fermentation technology, proving useful in the large scale expression of recombinant proteins in *E. coli*, and the production of antibiotic compounds [29,30].

In the present communication we report the crystal structure of recombinant ferric homodimeric VtHb, solved by a combination of single isomorphous replacement (SIR) methods and density modification techniques, and refined at 1.83 Å resolution. In addition, the 3D structure of the VtHb–azide complex has been studied at 1.76 Å resolution, at 100 K. The structure of VtHb is discussed in the light of its unusual heme distal ligand-binding site, its new quaternary assembly, and in relation to the structures of *Alcaligenes* flavoHb and homologous oxygen-binding heme proteins.

Results and discussion

Globin fold

Each VtHb subunit essentially conforms to the globin fold and to the general determinants of the globin structure organization [9,11]. Comparison of the mainchain protein structure in the two independent subunits of the homodimer yields a root mean square deviation (rmsd) of 0.18 Å. Sperm whale Mb [31] is often taken as the reference monomeric heme protein structure and shares 18% amino acid sequence identity with VtHb. Structural overlay of the VtHb subunit with sperm whale Mb [31] yields an rmsd of 1.6 Å, based on all mainchain atoms in the α-helical regions, and excluding the CD2–E9 segment. After polypeptide backbone superposition, the porphyrin group in the two hemoproteins adopts orientations differing by 9.5°. Moreover, in the case of VtHb, the heme is more deeply buried in its protein crevice (by about 1.5 Å).

A structural overlay of the α-helical segments of VtHb onto the globin domain of *Alcaligenes* flavoHb (51% amino acid sequence identity) yields an rmsd of 2.5 Å. Inspection of the superposed structures shows that the heme groups of the two proteins adopt a coplanar orientation, despite a deviation of 16° between their respective E helices (Fig. 1). If the E helices are omitted from the globin backbone superposition, the rmsd drops to 1.6 Å.

Helix organization

The A helix, covering residues Gln4(A2)–Glu19(A17), is kinked at Pro15(A13), an invariant residue in the known bacterial and yeast globin sequences (Fig. 2). A hydrophobic patch usually conserved in globin structures [32,33], provided by residues Ile7(A5), Ile10(A8) and Ile68, anchors the N-terminal helix to the EF corner. Transition from the A to the B helix occurs sharply at residue His20. Gly21(B2) starts the B helix, which extends to residue Lys35(B16). At site B6, the closest distance between the B and E helices, a glycine residue that is highly conserved in globin structures [11] is substituted in VtHb by Thr25(B6), which faces residue Lys55(E9). The presence of a medium size residue (i.e. Thr25) at site B6 does not, however, cause relative displacement of the B and E helices. Instead, the two helical backbones and the sidechain of Thr25(B6) create a surface pocket, which contains a highly ordered water molecule in both VtHb subunits (W203 and W204, respectively). W203 (and similarly W204) is hydrogen bonded with tetrahedral geometry to four atoms: Thr25(B6) OG1 (2.72 Å); the peptidic Lys55(E9) O (2.43 Å); Ala58(E12) N (2.97 Å); and Met59(E13) N (3.01 Å).

In the central part of the B helix, residue Phe28(B9) is oriented perpendicular to the phenolic ring of Tyr29(B10) (Figs 3a,b). The distance between the two aromatic rings (4 Å) may support electrostatic aromatic interactions between residues B9 and B10 [34]. Residue Tyr29(B10) protrudes into the heme distal site. The location of this residue is further defined by van der Waals contacts with Phe33(B14) and by a strong hydrogen bond between the Tyr29(B10) OH atom and the peptide O atom of residue Pro54(E8) (2.55 Å) (Figs 3a,b). The C-terminal part of helix B, together with the first half of the short C helix, is characterized by the presence of positively charged residues: Lys30(B11), Lys35(B16), His36(C1) and Arg40(C5). The C helix (a distorted 3_{10} helix covering residues 37–42)

Figure 1

Stereo view of the VtHb Cα backbone (thin lines) showing the remarkably different orientation adopted by the *Alcaligenes* flavoHb E helix (thick lines). For clarity, only the most divergent region of flavoHb, composed of the region between helices C and E (labeled in the picture), has been drawn. The 43–53 CE region, not observable in VtHb, adopts the conformation of an extended polypeptide in flavoHb. A full structural overlay of the two heme domains is shown in Figure 5. (The figure was drawn with MOLSCRIPT [68].)

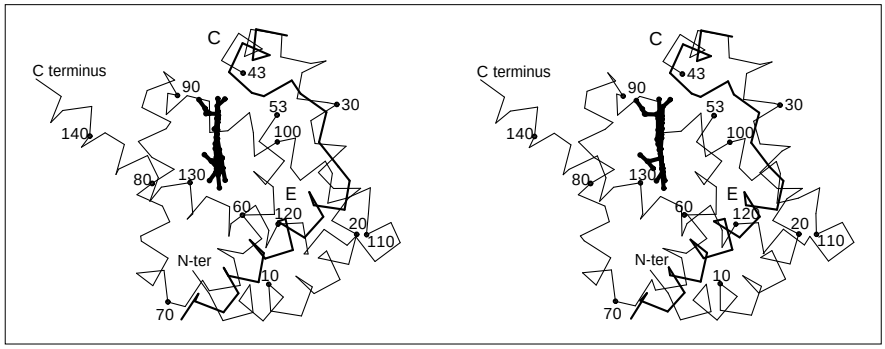

contains two proline residues, Pro37(C2) and Pro41(C6), the former is often a conserved proline residue in globins [6,11]. The role of the strictly invariant CD1 residue is played by Phe43, which is in van der Waals contact with the heme group next to the D pyrrole ring; the closest contact (3.58 Å) occurs with the heme CMD atom. Moreover, the Phe43(CD1) aromatic ring is perpendicular to the phenyl ring of Phe33(B14), and is located approximately 3.7 Å from it (Fig. 3a).

Following residue Phe43(CD1), the electron density of the polypeptide chain is sharply interrupted and missing for a stretch covering residues Asp44–Glu52, in both subunits. At residue Gln53(E7) the electron density is well defined and the polypeptide chain leading to the E helix can be clearly traced. Nevertheless, a regular α-helical structure is properly attained only at residue Leu57(E11), and extends through to Glu66(E20). The expected distal residue Gln53(E7), invariant in all known bacterial and

Figure 2

```
                    1        10        20        30        40        50        60        70
Vitreoscilla        MLDQQTINIIKATVPVLKEHGVTITTTFYKNLFAKHPEVRPLFDMGRQESLEQPKALAMTVLAAAQNIENLPA
B.subtilis          MLDNKTIEIIKSTVPVLQQHGETITGRFYDRMFQDHPELLNIFNQTNQKKKTQRTALANAVIAAAANIDQLGN
S.cerevisiae        MLAEKTRSIIKATVPVLEQQGTVITRTFYKNMLTEHTELLNIFNRTNQKVGAQPNALATTVLAAAKNIDDLSV
A.eutrophus         MLTQKTKDIVKATAPVLAEHGYDIIKCFYQRMFEAHPELKNVFNMAHQEQGQQQQALARAVYAYAENIEDPNS
E.chrysanthemi      MLDQQTIATIKSTIPLLAETGPALTAHFYQRMFHHNPELKDIFNMSNQRNGDQREALFNAICAYATHIENLPA
E.coli              MLDAQTIATVKATIPLLVETGPKLTAHFYDRMFTHNPELKEIFNMSNQRNGDQREALFNAIAAYASNIENLPA
V.parahaemolitycus MLSNQTIEIVKATAPLIAETGPKLTAHFYDRMFTHNPELKDIFNMSNQRNGDQREALFNAICAYAANIENLPA
P.norvegensis       MLTPTEINFLQSLAPVVKEHGVTVTSTMYKYMFQTYPEVRSYFNMTNQKTGRQPKVLAFSLYQYILHLNDLTP
                       |<-----A------>| |<-----B----->| |<C >|             |<--E--->|
                       A2         A13   B2      B10           CD1       E7  E11


                            80        90        100       110       120       130       140
Vitreoscilla        ILPAVKKIAVKHCQAGVAAAHYPIVGQELLGAIKEVLGDAATDDILDAWGKAYGVIADVFIQVEADLYAQAVE
B.subtilis          IIPVVKQIGHKHRSIGIKPEHYPIVGKYLLIAIKDVLGDAATPDIMQAWEKAYGVIADAFIGIEKDMYEQAEE
S.cerevisiae        LMDHVKQIGHKHRALQIKPEHYPIVGEYLLKAIKEVLGDAATPEIINAWGEAYQAIADIFITVEKKMYEEAL
A.eutrophus         LMAVLKNIANKHASLGVKPEQYPIVGEHLLAAIKEVLGNAATDDIISAWAQAYGNLADVLMGMESELYERSAE
E.chrysanthemi      LLPAVERIAQKHASFNIQPEQYQIVGTHLLATLEEMF--QPGQAVLDAWGKRYGVLANVFIQRESDIYQQSAG
E.coli              LLPAVEKIAQKHTSFQIKPEQYNIVGEHLLATLDEMF--SPGQEVLDAWGKAYGVLANVFINREAEIYNENAS
V.parahaemolitycus LLGAVEKIAHKHTSFLITKDQYQIVGKHLIATIDELF--NPGQEVLGAWAEAYGVLANVFIQREEQIYQANAS
P.norvegensis       ISGFVNQIVLKHCGLGIKPDQYPVVGESLVQAFKMVLGEAADEHFVEVFKKAYGNLAQTLIDAEASVYKTL
                     |<----F-----><|      |<-----G------>|     |<------------H----------->|
                        F1    F8         G5                   H2        H12        H23
```

Amino acid sequence alignment of VtHb with known related bacterial and yeast globin domains. The sequences are arranged in order of decreasing amino acid sequence identity, with respect to VtHb. The multiple alignment has been achieved using the program CLUSTAL V [69], and based on 3D structural considerations in the case of VtHb and flavoHb, for the assignment of the topological positions. The topological regions are marked below the sequences according to the standard globin fold nomenclature. Amino acid numbering refers to the VtHb sequence. The span of the helical regions in VtHb has been marked with vertical bars at the topological position of the first helical residue. Residues which are fully invariant in the eight aligned sequences have been represented by bold characters.

Figure 3

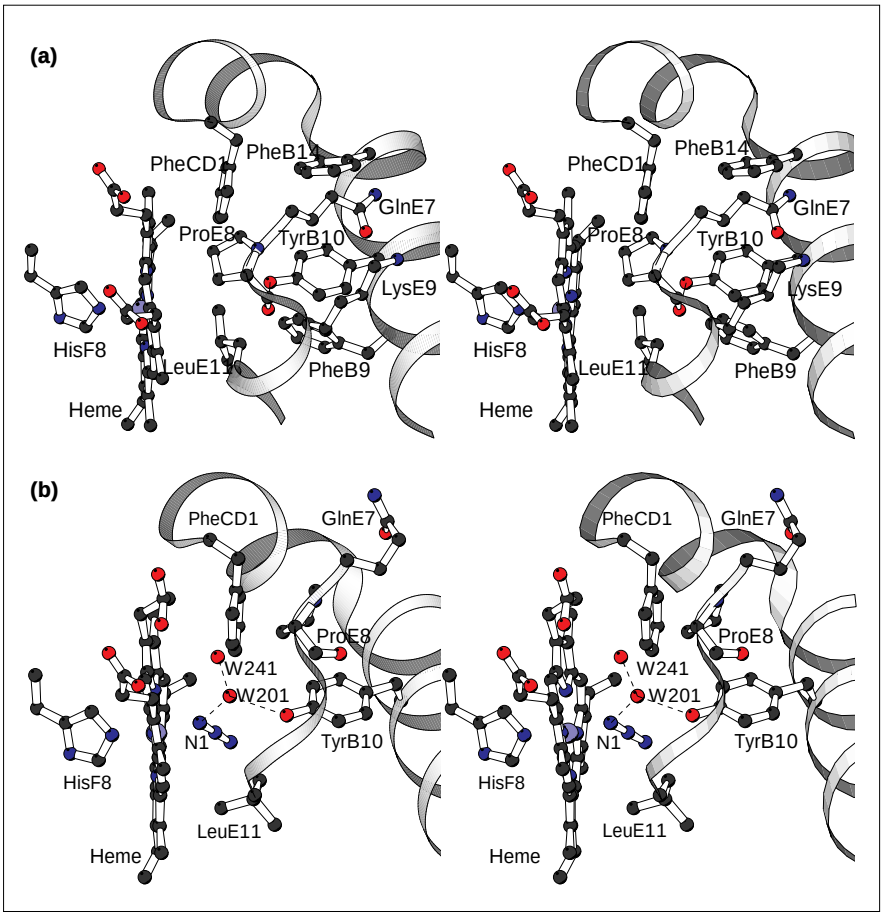

Conformational transitions in the VtHb heme distal site region. **(a)** Stereo view of the heme pocket in ligand-free ferric VtHb, showing the crowding of residues in the distal site. In this view the protein molecule is approximately oriented as in Figure 1. Portions of the B and C helices are shown as a ribbon representation in the background. The pre-E region, supporting Gln53(E7) and Pro54(E8), and the proximal His85(F8) residue are also shown. **(b)** Stereo view of the distal site in the VtHb–azide complex, showing the remarkable structural rearrangement of the distal site residues Tyr29(B10), Glu53(E7), Pro54(E8) and Leu57(E11). The ligand is coordinated to the heme iron through its N1 atom and hydrogen bonded to the bridging water molecule W201; hydrogen bonds are represented by dashed lines. Oxygen atoms are drawn in red, nitrogen atoms in dark blue and the iron atom is shown as a pale blue sphere. (The figure was drawn using the program MOLSCRIPT [68].)

yeast globin amino acid sequences (Fig. 2), is oriented towards the solvent, away from the expected ligand-binding site. This residue is engaged in two hydrogen bonds with Lys55(E9): Gln53(E7) O–Lys55(E9) N (2.50 Å); and Gln53(E7) OE1–Lys55(E9) NZ (3.14 Å) (Fig 3a). At position E8 residue Pro54 prevents access of the solvent or ligand to the heme distal site by directly contacting both the porphyrin ring (through the Pro54(E8) CB and CD atoms) and Phe43(CD1) (through the Pro54(E8) CD atom). Moreover, the carbonyl O atom of Pro54(E8) is hydrogen bonded to Tyr29(B10) OH, thus yielding an unusual ϕ,ψ pair value (–68°, 93.4°) for a proline residue. Leu57(E11), as regularly observed at this topological site, is in contact with the lower part of the porphyrin ring, achieving a distance of 3.85 Å between atom 57(E11) CG and the heme CHB methinic bridge. Moreover, the sidechain orientation brings atom 57(E11) CD1 to a distance 3.72 Å from the heme iron atom, filling a good part of the potential distal ligand-binding site (compare Figs 3a and 3b).

The EF corner contains two turns of a 3_{10} helical segment, and comprises residues Ile68–Ala73. Within the globin fold the EF corner is followed by the F helix (comprising residues Leu75–Ala88(F11)); residue Ile81(F4) contacts the heme on the proximal side, opposite to Leu57(E11). The imidazole ring of the proximal His85(F8) is coordinated to the heme iron (2.05 Å), and kept in its azimuthal orientation with respect to the heme pyrrole nitrogen atoms. This orientation is maintained by hydrogen bonding of His85(F8) ND1 to two atoms: Tyr95(G5) OH (3.09 Å) and Glu137(H23) OE2 (2.63 Å) (Fig. 4). Both Tyr95(G5) and Glu137(H23) are invariant residues in bacterial and yeast globin amino acid sequences (Fig. 2), and are mutually connected by a hydrogen bond between atoms Tyr95(G5) OH and Glu137(H23) OE1 (2.67 Å). A very similar hydrogen-bonding network involving residues His85(F8), Tyr95(G5) and Glu137(H23) has been observed in *Alcaligenes* flavoHb [14]. The His85(F8) imidazole ring forms an angle of about 5° with respect to the heme pyrrole NB-ND direction. This orientation differs by about 90° from that commonly adopted in vertebrate and invertebrate globin structures, but is almost coincident with that of HisF8 in *Alcaligenes* flavoHb [14,35]. The FG region and the G helix (residues Tyr95(G5)–Leu110(G20)) provide

Figure 4

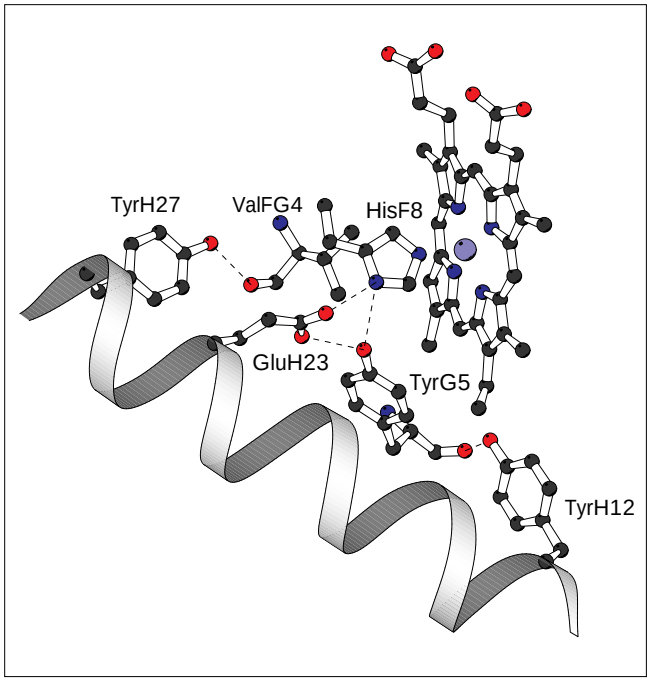

Details of the heme pocket proximal site in VtHb, including His85(F8) and the hydrogen-bonded residues which define its azimuthal orientation with respect to the heme plane; part of the H helix is shown as a ribbon. Hydrogen bonds are represented by dashed lines; color-coding is as described in Figure 3. (The figure was drawn using the program MOLSCRIPT [68].)

Figure 5

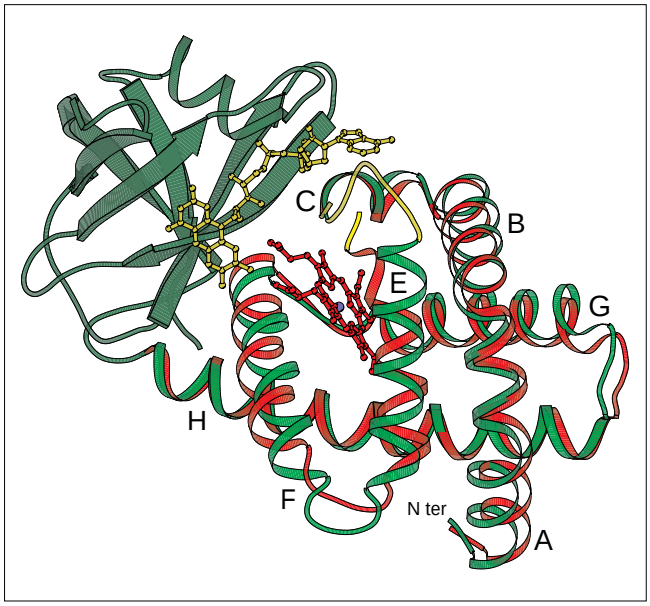

A structural overlay of one VtHb subunit (red) onto the 1–272 region of *Alcaligenes* flavoHb, comprising the heme domain (green) and the FAD-binding region in the C-terminal domain (dark green). For clarity, only the heme group of VtHb is shown, and the NADP-binding region of flavoHb (residues 273–403) is not shown. The adenine portion of FAD (yellow) in the upper part of the picture, points towards the CE regions of flavoHb (yellow) and towards the 9-residue disordered CE segment of VtHb. (The figure was drawn using the program MOLSCRIPT [68].)

the heme contacting residues: Val90(FG4) (opposite to Phe43(CD1) on the heme proximal face), Tyr95(G5) and Val98(G8).

In *Alcaligenes* flavoHb, the H helix was observed to lead into the flavin domain, similarly this helix covering residues Glu116(H2)–Gln143(H29) is also rather extended in VtHb (Figs 1,5). Helix H includes the only tryptophan residue present in VtHb, at position H8, which is engaged in a hydrogen bond to Thr13(A11) OG1 (2.93 Å). In addition, Tyr126(H12) OH is hydrogen bonded to the peptide O atom of Tyr95(G5) (2.66 Å), and Tyr141(H27) OH is hydrogen bonded to the peptide O atom of Val90(FG4) (2.58 Å) (Fig. 4). The latter interaction, adjacent to the Val90(FG4) sidechain contact with the heme ring, is reminiscent of the intramolecular hydrogen bond whose loosening is at the basis of the T→R transition in mammalian Hbs [9,36]. The C-terminal region of helix H contacts helix F through a series of juxtaposed sidechains, which form a sort of hydrophobic zipper motif. The residues involved (Ile68, Leu71, Leu75, the aliphatic part of Lys79(F2), Val83(F6), Ile129(H15), Val132(H18), Val136(H22) and Leu140(H26)) are essentially conserved in known bacterial and yeast globin domains (Figs 2,6), and partly build the subunit association interface in the VtHb homodimer.

The CE region and the distal site

As described above, the protein region following residues Phe43(CD1) and leading to helix E is disordered in both VtHb subunits. Inspection of the amino acid sequences of the aligned bacterial and yeast globin domains shows that the disordered CE region of VtHb is rich in negatively charged residues (Asp44, Glu49 and Glu52), as opposed to an overall neutral or positively charged area observed in the other sequences listed in Figure 2. Moreover, residue Gly46 is unique to VtHb and may increase the structural flexibility of this region.

In *Alcaligenes* flavoHb, the CE region of the heme domain displays higher than average temperature factors with poorly defined sidechain electron density [14]. It adopts an extended conformation and is in contact, and hydrogen bonded, with the adenine portion of FAD through residues His47 and Gln48 (Arg47 and Gln48 in VtHb, respectively) (Figs 1,5). A glutamine residue at position 48 is fully conserved in the nine known bacterial and yeast globin domains (Fig. 2), suggesting a functional or key structural role for this residue.

Despite the lack of proper secondary structure for residues E7–E10, the location of the E11–E20 helical segment

Figure 6

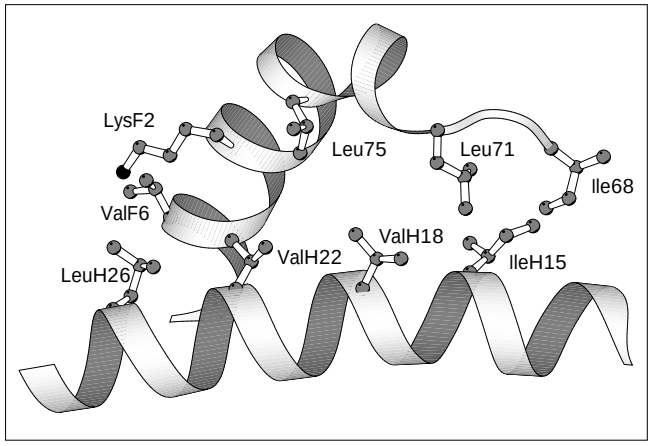

A ribbon drawing of the intramolecular hydrophobic zipper observed in VtHb, between helices F and H, which also builds the intersubunit contact region. (The figure was drawn using the program MOLSCRIPT [68].)

allows contacts between the distal residues Pro54(E8), Leu57(E11), Thr60(E14), Val61(E15) and the porphyrin ring. On the contrary, due to the unusual orientation of the E helix, no direct heme–protein contacts occur along the E helix in *Alcaligenes* flavoHb [14] (Figs 1,5). This substantial structural difference, among two globin domains sharing 51% amino acid identity, may suggest that the presence of the flavin-binding domain in *Alcaligenes* flavoHb is reflected by a conformational transition in the CE region of this protein. Conversely, the absence of such a molecular partner (and of related contacts) in the VtHb homodimer may be the basis of the structural flexibility displayed by the CE region. In this context it should be noted that a NADH-dependent FAD-containing reductase, which copurifies with the native VtHb, has been isolated from *Vitreoscilla* sp. and partly characterized. This flavoprotein has been proposed to be the natural reducing agent for the heme domain of VtHb [37–39].

The irregular (but defined) structure of the E7–E10 distal site region is totally unexpected, as this region of the globin fold has been observed in an α-helical conformation in all structures known so far. The unusual conformation of the E7–E10 region in VtHb is stabilized by three hydrogen bonds (involving Tyr29(B10), Gln53(E7), Pro54(E8) and Lys55(E9); see above and Fig. 3a), and may partly reflect the presence of residues Leu51, which is almost invariantly a glycine residue in the bacterial and yeast sequences (Fig. 2), and of Pro54(E8), which starts the following α-helical segment. Moreover, crystal contacts between residue Gln53(E7) and the FG region of a symmetry-related molecule may additionally perturb the E7–E10 local conformation observed in both VtHb subunits.

Structure of the liganded distal site

A glutamine residue, substituting for the highly conserved histidine residue at the distal topological position E7, is scarcely observed in vertebrate globins [11]. Gln(E7) is more abundantly represented in nonvertebrate hemoproteins, and is invariant in the known bacterial and yeast heme domain sequences (Fig. 2). When the GlnE7 residue is supported by a regular α-helical E segment, the sidechain can fold into the heme distal site and stabilize the bound ligand through hydrogen bonding. Stabilization of the ligand through a distal glutamine has been observed in elephant Mb [40], in engineered sperm whale Mbs [41], in *Lucina pectinata* HbI [42] and in *Ascaris suum* isolated D1 heme domain [43,44]. Moreover, the additional contribution of residue B10 (either phenylalanine or tyrosine), has been shown to affect dioxygen affinity through the electrostatic interaction of the aromatic protons or through hydrogen bonding, respectively. This effect has been observed in elephant Mb [40], in the engineered Leu(B10)→Phe and Leu(B10)→Tyr sperm whale Mb mutants [45–47], and in the *A. suum* D1 heme domain [43,44]. In particular, these studies have shown that very low ligand dissociation rate constants can be achieved only when the Tyr(B10) hydroxyl is properly positioned in the heme distal site. The correct positioning is achieved by the formation of hydrogen bonds with the iron-coordinated dioxygen as well as with the Gln(E7) sidechain.

Binding of azide to VtHb results in structural changes which are mainly centered at the two heme distal sites. The anionic azide ligand is coordinated to the heme iron atom (the Fe–ligand coordination bonds are 1.98 Å and 2.01 Å, in the two subunits) and is oriented towards the back (hydrophobic) region of the heme crevice (Fig. 3b). The Fe–ligand angle (Fe–N1–N3 in Fig. 3b) is 112° and 124°, in the two VtHb subunits. Upon azide binding, the iron atom in both subunits is shifted towards the heme plane by 0.25 Å, from an out of plane location of 0.27 Å observed in the ligand-free protein. Such a coordination geometry is reminiscent of the observed binding mode of azide to ferric sperm whale Mb [48–50]. In the ligand-free protein, azide access to the distal site is prevented by contacts made by residue Pro54(E8) with the heme, with Phe43(CD1) and Leu57(E11). Moreover, a potential secondary ligand access route pointing to the heme distal site through the disordered CE region may be interrupted by the phenolic ring of Tyr29(B10), which is hydrogen bonded to the carbonyl O atom of Pro54(E8).

Upon azide binding, Pro54(E8) is shifted by 3.0 Å from its heme contacting position (through a ψ angle increase of about 60°), opening access for two water molecules (W201 and W241, with B factors of 15.7 $Å^2$ and 26.2 $Å^2$, respectively) which fill the distal site together with the ligand (Fig. 3b). Reflecting the hydrogen bonds and tight distal site residue packing present in the ligand-free protein,

the conformational readjustment of residue Pro54(E8) is coupled to the reorientation of the Leu57(E11) and Tyr29(B10) sidechains, which move by about 1.5 Å each. In both VtHb subunits Tyr29(B10) OH forms a hydrogen bond to W201 (2.65 Å), which, in turn, is hydrogen bonded to the iron-coordinated azide N1 atom (2.50 Å) and to W241 (2.98 Å) (Fig. 3b). The free end of the ligand (N3 atom) is located approximately over the C1C heme atom, contacting residues Phe43(CD1), Phe28(B9) and Leu57(E11).

The crystal structure of the VtHb–azide complex shows interpretable electron density for Glu52(E6) and Glu146 residues, in both subunits. Moreover electron density for the residues Leu2 and Leu51(E5) can be recognized in one subunit. The E5–E10 segment, nevertheless, maintains an extended irregular polypeptide conformation. It should be noted that the observation of electron density for these additional residues in the VtHb–azide complex may result from the cryocooling of the crystal during data collection.

Homodimeric assembly

The quaternary structure of the VtHb homodimer shows a new assembly rule for globin domains (Fig. 7). The intersubunit contact region is defined by a sort of loose and tilted four-helical bundle, based essentially on the juxtaposition of helices F and H from each subunit. Contrary to a conventional α-helical bundle, however, the interacting helices, related in VtHb by the local twofold axis, are not antiparallel. The intersubunit contact buries a molecular region defined by residues Gln69, Asn70, Pro72, Ala73, Leu75 and Pro76 in the N-terminal part of the F helix (often called the pre-F helix), and by residues Asp131(H17), Val132(H18), Gln135(H21), Val136(H22) and Asp139(H25), in each VtHb subunit. Moreover, the N termini of the two subunits are close to each other, with residues Leu2, Glu4(A2) and Ile7(A5), within 5 Å from their counterparts in the opposing subunit.

The main intersubunit contact zone in the VtHb homodimer is based on a molecular interface area of 434 Å^2, a rather contained value if compared to the values generally observed for other protein–protein interface areas [51], and more specifically to the other quaternary assemblies observed in the globin family. As a comparison, the subunit interfaces in the dimeric cooperative Hbs from the mollusc *Scapharca inequivalvis* and from the echinoderm *Caudina arenicola*, both based on contacts between the E–F helices of two opposing subunits, are about 2000 Å^2 [52,53]. Moreover, in the homotetrameric (non-cooperative) Hb from the marine worm *Urechis caupo*, the subunit interfaces display areas of 710Å^2 and 730Å^2, and are based on contacts involving the A–B turn and E helices, or the G–H turn and D helices, respectively [54].

Intersubunit association in VtHb is essentially based on van der Waals contacts, and includes four water molecules (two pairs related by the local twofold axis crossing the subunit interface) acting as hydrogen-bonded bridges between residues Ala73–Asp139′ and Pro72–Asp139′. The subunit contact based on the assembly of the F–H helix pairs defines a solvent inaccessible cavity of 86 Å^3. Although the intermolecular interface area is contained it involves portions of the F and H helices. Thus, this interface is a good candidate for the transfer of conformational effects, which, upon ligand binding, are transmitted through the proximal F8 histidine to helix F and to the rest of the molecular assembly. Nevertheless, the 3D structures reported here show that a movement of the Fe atom by 0.25 Å into the heme plane (upon azide binding) has a contained effect on the quaternary structure of VtHb. The rmsd calculated over the mainchain atoms of ligand-free (room temperature data) and azide-bound (100 K data) homodimers is 0.65 Å.

Figure 7

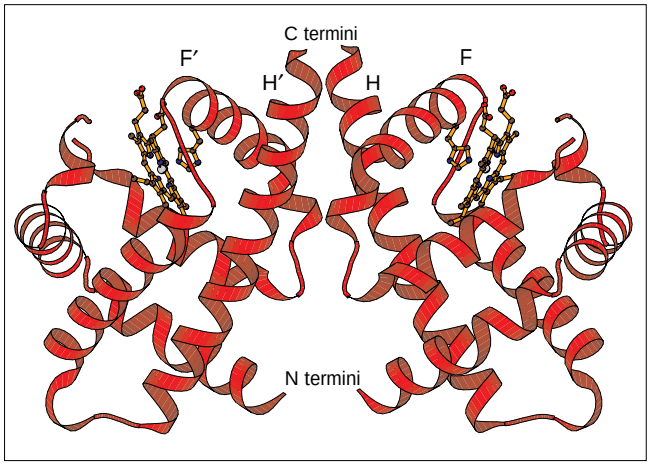

A view of the quaternary assembly in the VtHb homodimer. The view shows the molecular interface based on portions of the F and H helices (see labels) bundled around the local twofold axis (almost vertical in the drawing). The heme groups (orange) and the proximal His85(F8) residues are shown. (The figure was drawn using the program MOLSCRIPT [68].)

Conclusions

The existing literature on ligand binding to VtHb reports cooperativity in carbon monoxide and cyanide binding, as well as inequivalence in the binding properties of the two heme domains [2,24–27]. However, the structure of the VtHb–azide complex, determined using recombinant protein in the presence of saturating concentrations of ligand, does not indicate differential azide binding nor significant quaternary structure transitions. Analysis of the ferrous and ferric protein in the presence/absence of gaseous diatomic ligands and cyanide, as well as extensive study of the kinetic properties of the recombinant homodimeric VtHb, will be required before more light can be shed on these aspects.

Concerning the efficiency of azide recognition by ferric VtHb, it can be noted that the ligand-free distal site is incorrectly structured to accept an incoming ligand, as conformational changes are clearly required to make the sixth iron-coordination position accessible (Fig. 3). Nevertheless, the azide association rate constant for VtHb ($k_{on} > 3\times10^5 M^{-1} s^{-1}$, pH 7.0, 22.0°C; M Coletta and PA, unpublished results) is higher than that observed for wild type (HisE7) sperm whale Mb ($k_{on} = 3.1\times10^3 M^{-1} s^{-1}$, pH 7.0, 22.0°C), which displays an iron-coordinated water molecule at the distal site [31,41,55]. This observation was made for *Aplysia limacina* Mb ($k_{on} = 2x10^6 M^{-1} s^{-1}$; [50]) and for ValE7 or LeuE7 sperm whale Mb mutants, lacking an iron-coordinated water molecule [33,41,55].

In the crystal structure of the isolated D1 domain of *A. suum* Hb, the dioxygen molecule (coordinated to the heme iron) is buried in the distal site, and stabilized by direct hydrogen bonds to both TyrB10 and GlnE7. These two residues, in turn, are mutually hydrogen bonded. In the VtHb–azide complex — formally displaying the same distal site residues, TyrB10 and GlnE7, as the *A. suum* D1 domain — the ligand is stabilized in its coordination site only by one water-mediated hydrogen bond to Tyr29(B10). This structural organization may form the basis of the observed VtHb azide dissociation rate constant ($k_{off} > 100 s^{-1}$, pH 7.0, 22.0°C; M Coletta and PA, unpublished results), which is faster than that observed in wild type sperm whale Mb ($k_{off} = 0.12 s^{-1}$, pH 7.0, 22.0°C) [55]. Thus, the VtHb structure confirms that, despite the conservation of the globin fold and the identical nature of key residues in the globin distal sites, the precise juxtaposition of their sidechains (supported by α-helices or polypeptide backbones of slightly different orientations and packings) plays a fundamental role in regulating ligand recognition processes and affinity [47].

Finally, considering the different (and beneficial) roles which have been attributed to VtHb, it could be argued that the protein may be present *in vivo* in two functional states. In the homodimeric form, analyzed here, the unusual distal site structure allows oxygen binding, possibly facilitating oxygen diffusion within the cellular (and periplasmic) environment. A hypothetical heterodimeric form of VtHb (composed of one heme binding subunit and one NADH-dependent flavoprotein reductase subunit) has been proposed. In this heterodimeric form of VtHb, the protein may conform to a flavoHb-like structural organization, achieving cellular functions similar to those played by the single chain flavoHb isolated from bacteria and yeast [37–39].

Biological implications

The discovery in bacteria and yeast of chimeric proteins which contain a heme domain has not been followed by definitive functional assignments. In some higher organisms, O_2, NO and CO sensor proteins have been proposed to be based on the coupling of heme and flavoprotein (or kinase) domains. Hemoglobin from the bacterium *Vitreoscilla* sp. (VtHb), is a homodimeric globin devoid of any covalently linked flavin domains. VtHb, however, is structurally related to bacterial and yeast flavohemoglobin (flavoHb) heme domains, sharing 43–56% amino acid sequence identity. In the strictly aerobic bacterium *Vitreoscilla* sp., expression of the protein is strongly induced by a decrease in O_2 levels. VtHb has been proposed to facilitate oxygen diffusion to the bacterial terminal oxidases.

The crystal structure of recombinant VtHb is shown to exhibit the characteristic globin fold, despite the very low sequence homology to vertebrate hemoglobins. The subunit interface in the functional homodimer is based on a small contact area (434 Å^2), defined by segments of two opposing helices (F and H) in each subunit. The interface forms a previously undescribed quaternary assembly, which is unaltered by azide binding. The structural organization of the VtHb distal (ligand-binding) site is unique within the globin family. The region encompassing the CD segment, the D helix and part of helix E are disordered, and the residues between the globin topological positions E7 and E10 do not adopt the expected α-helical conformation, such that substantial conformational changes are required in order to allow access to the incoming ligand. The crystal structure analyzed here shows that the key residue involved in azide binding to the distal site is Tyr29 (located on helix B) in the inner part of the heme cavity. The distal site conformational transition and the detailed mechanism of ligand recognition and binding have little in common with the related processes known for vertebrate globins. This is in agreement with the reported much wider variability of structure and functionality among nonvertebrate globins. It also supports the concept of functional adaptability of the globin fold, which, despite the remarkable conservation ot the three-on-three helical sandwich motif, allows (in different species) recognition/discrimination of diatomic ligands, and modulation of dioxygen affinity over a range of four orders of magnitude.

Absence of a defined structure in the region between the C and E helices of VtHb may reflect the lack of intramolecular interactions with the FAD group of a coupled flavin domain. The discovery of a NADH-dependent flavin reductase in *Vitreoscilla* sp. suggests that the heme and the flavin domains have separated in this bacterium during evolution. Nevertheless, very little is known about the specificity of their interaction. Considering the high level of primary structure conservation among bacterial globin domains, the crystal structure of VtHb will help in understanding the molecular models and the ligand-binding processes of its

homologs. Moreover, given the increased activity of *Escherichia coli* terminal oxidases induced by heterologous expression of VtHb, it may support the design of mutants for applications in fermentation technology.

Materials and methods

Expression, purification and crystallization

The VtHb gene was cloned and overexpressed in *E. coli.* VtHb was purified as previously described [56]. Crystals of the ferric form of VtHb were grown from 1.3 M ammonium sulfate, 0.1 M pyrophosphate buffer pH 6.4, 3% v/v ethylene glycol. VtHb crystals belong to the monoclinic $P2_1$ space group, with unit cell constants: a = 62.9, b = 42.5, c = 63.2 Å, $\beta = 106.6°$. There is one homodimer per asymmetric unit. Crystals of the VtHb–azide complex were prepared by soaking the native ferric protein crystals at room temperature for 1 h in their mother liquor supplemented with 18% v/v glycerol as cryoprotectant, and containing 0.03 M sodium azide, at pH 7.0.

Data collection and structure solution

A high-resolution VtHb native data set was collected at LURE (Laboratoire pour l'Utilization de la Radiation Electromagnétique, Paris, France), in an attempt to use Xe atoms for isomorphous replacement. Two data sets (in the 25.0 Å–1.83 Å resolution range) were collected on the same crystal: at 15 bar Xe pressure, and in its regular mother liquor. 42 X-ray diffraction data sets, at about 2.5 Å resolution, were collected in house using a Rigaku R-axis IIc image plate system in an extensive screen for potential heavy atoms derivatives. Diffraction data for the VtHb–azide complex were collected at the ELETTRA synchrotron radiation diffraction line (Trieste, Italy), using a 180 mm Mar-Research image plate system, at 100 K, on one crystal (Table 1). The MOSFLM and CCP4 packages [57,58] were used for the data reduction and handling throughout.

Calculation of the VtHb self-rotation function (in the 10Å–3.0 Å resolution range) showed a prominent peak located at $\varphi = 0°$, $\psi = 36°$, $\kappa = 180°$, in keeping with the strong pseudo-orthorhombic symmetry of the diffraction pattern [56].

Attempts to solve the VtHb 3D structure by molecular replacement, based on various eukaryotic Hb or Mb models, failed to produce consistent results. This was also unexpectedly the case when the *Alcaligenes* flavoHb heme domain [14] was used as a search model, despite the 51% amino acid sequence identity relating this domain to VtHb. Trimmed or partial models of most globins in the Brookhaven Protein Data Bank [59] were also considered in an extensive, but unsuccessful, molecular replacement search, which was therefore abandoned.

Structure solution was subsequently pursued through isomorphous replacement techniques. Binding of Xe to the globin was not detectable, as evaluated by means of difference Patterson techniques based on the data collected at 15 bar Xe pressure. Nevertheless, the crystal used for the native data set collection at LURE (Table 1) proved highly isomorphous with respect to a VtHb $Au(CN)_2$ derivative previously collected in house (soaking conditions: 0.6 mM, pH 6.4, 1 week), yielding interpretable difference Patterson maps using SHELX90 [60]. A SIR phased map, calculated at 2.1 Å resolution and based on this derivative, was of sufficient quality to locate the molecular boundaries for the dimer and to show the iron-atom locations as the two highest features in the electron density. Moreover, inspection of the anomalous difference Fourier maps provided the correct hand assignment for the heavy-atom sites.

The starting map was improved by means of density modification techniques, using the 'solvent flipping' approach of Abrahams [61] in the 25.0Å–2.1 Å resolution range. The electron density for the heme group and five helices in each subunit (after density modification) were then used as a guide for the fitting of the *Alcaligenes* flavoHb heme domain atomic model to the VtHb density. Individual helices, with the exception of helix E, were refined as independent rigid bodies using X-PLOR 3.1 [62], achieving R factor value of 48% (at 3.0 Å resolution). This preliminary model was used to calculate a molecular envelope with the program NCSMASK [58]. Refinement of the molecular twofold axis orientation and position was achieved using the program GLRF [63], based on the SIR-phased and solvent-flattened map and the twofold

Table 2

Refinement statistics.

	Native (room temperature)	Azide complex (100K)
Resolution (Å)	25.0–1.83	15.0–1.76
No. of protein atoms	2149	2167
No. of solvent atoms	123	183
R factor (%)	18.8	20.3
R free (%)*	25.5	26.3
$\Delta C\alpha$ (Å)†	0.18	0.35
B factor mainchain (Å^2)	30.0	23.0
B factor sidechain (Å^2)	41.0	30.0
B factor solvent (Å^2)	48.6	47.9
‡Ramachandran plot		
core region (%)	96.2	95.8
Allowed region (%)	3.8	4.2
Disallowed region (%)	0.0	0.0
Rmsd from ideality		
bond lengths (Å)	0.012	0.014
bond angles (°)	2.26	2.12
B factor bonded atoms (Å^2)	5.8	7.0

*R free = $\Sigma \mid F_{obs} - F_{calc} \mid / \Sigma \mid F_{obs} \mid$ (for 4% of all the data). †Root mean square deviation (rmsd) for all Cα atoms after superposition of the two subunits. ‡Values determined according to PROCHECK [67].

Table 1

Data collection and phasing statistics.

Crystal	X-ray source	Resolution (Å)	Measurements	Independent reflections	Completeness (%)	R_{merge}* (%)	R_{iso}† (%)	Phasing power	Figure of merit‡
Native	BW21B LURE	25.0–1.83	101 071	26 949	95.3	5.5	–	–	–
$Au(CN)_2$	Rigaku RU200HB	20.0–2.10	46 832	15 069	71.0‡	6.1	18.7	1.4	0.35
NaN_3	XRD ELETTRA	15.0–1.76	68 840	27 536	91.5	4.9	–	–	–

*$R_{merge} = \Sigma \mid Ii - < Ii > \mid / \Sigma < Ii >$, where $< Ii >$ is the mean value of the ith intensity measurements. †$R_{iso} = \Sigma \mid \mid F_{ph} \mid - \mid F_p \mid \mid / \Sigma \mid F_p \mid$, where F_{ph} and F_p are the derivative and native structure factors, respectively. ‡90% complete in the 20.0–2.4 Å resolution range.

axis orientation obtained from the self rotation function. Electron density averaging around the local twofold axis, using the program DM [58], brought an appreciable improvement in the electron-density map.

Model building and refinement

Analysis of the averaged electron-density map allowed model building of the heme group together with 80% of the VtHb molecule (R factor 34.6%, for the data in the 25.0Å–2.1 Å resolution range; R free 41.1%). Model and experimental phases were combined using SIGMAA [64]; the resulting map showed the rest of the molecule, apart from the disordered CE region between residues 44 and 52. The model was then refined by iterated use of graphical sessions, using O [65] and TNT without any NCS restraints [66] (final R factor 18.8%, for the data in the 25.0Å–1.83 Å resolution range; R free 25.5%) (Table 2). The structure of the VtHb–azide complex was subsequently analyzed by means of difference Fourier techniques starting from the refined native VtHb model, and refined using the program O and programs from the TNT package.

Accession numbers

Atomic coordinates of both native ferric VtHb and the VtHb–azide complex, together with structure factors, have been deposited with the Brookhaven Protein Data Bank (coordinates accession codes 1VHB and 2VHB, respectively) [59].

Acknowledgements

We are grateful to A Mattevi and M Rizzi (Pavia) and C Travaglini-Allocatelli (Rome) for helpful advice and discussion. We also thank R Fourme and M Schiltz for helpful assistance during data collection at LURE, U Ermler (Max-Plank-Institut für Biophysik, Frankfurt, Germany) for making available the coordinates of the flavoHb from *Alcaligenes eutrophus*, and M Coletta for the functional characterization of the VtHb–azide complex. Part of this work was supported by the European Union Human Capital Mobility Program contract 94-0690.

References

1. Perutz, M.F. (1990). Mechanisms regulating the reactions of human hemoglobin with oxygen and carbon monoxide. *Annu. Rev. Physiol.* **52**, 1–25.
2. Wittenberg, J.B. & Wittenberg, B.A. (1990). Mechanisms of cytoplasmic hemoglobin and myoglobin function. *Annu. Rev. Biophys. Chem.* **19**, 217–241.
3. Takagi, T. (1993). Hemoglobins from single-celled organisms. *Curr. Opin. Struct. Biol.* **3**, 413–418.
4. Andersson, C.R., Ostergaard, E.O., Llewellyn, D.J., Dennis, E.S. & Peacock, W.J. (1996). A new hemoglobin gene from soybean: a role for hemoglobin in all plants. *Proc. Natl. Acad. Sci. USA* **93**, 5682–5687.
5. Vinogradov, S., *et al.,* & Trotman, C.N.A. (1993). Adventitious variability? The amino acid sequences of nonvertebrate globins. *Comp. Biochem. Physiol.* **106**, 1–26.
6. Kapp, O.H., Moens, L., Vanfletern, J.R., Trotman, C.N.A., Suzuki, T. & Vinogradov, S. (1995). Alignment of 700 globin sequences: extent of amino acid substitution and its correlation with variation in volume. *Protein Sci.* **4**, 2179–2190.
7. Hardison, R.C. (1996). A brief history of hemoglobins: plant, animal, protist, and bacteria. *Proc. Natl. Acad. Sci. USA* **93**, 5675–5679.
8. Moens, L., *et al.,* & Vinogradov, S. (1996). Globins in nonvertebrate species: dispersal horizontal gene transfer and evolution of the structure-function relationship. *Mol. Biol. Evol.* **13**, 324–333.
9. Perutz, M.F. (1979). Regulation of oxygen affinity of hemoglobin: Influence of structure of the globin on the heme iron. *Annu. Rev. Biochem.* **48**, 327–386.
10. Dickerson, R.E. & Geis, I. (1983). *Haemoglobin.* The Benjamin/Cummings Publishing Co., Menlo Park, CA, USA.
11. Bashford, D., Chothia, C. & Lesk, A.M. (1987). Determinants of a protein fold. Unique features of the globin amino acid sequences. *J. Mol. Biol.* **196**, 199–216.
12. Andrews, S.C., Shipley, D., Keen, J.N., Findlay, J.B.C., Harrison, P.M. & Guest, J.R. (1992). The hemoglobin-like protein (HMP) of *Escherichia coli* has ferrisiderophore reductase activity and its C-terminal domain shares homology with ferredoxin $NADP^+$ reductase. *FEBS Lett.* **302**, 247–252.
13. Zhu, H. & Riggs, A.F. (1992). Yeast flavohemoglobin is an ancient protein related to globins and a reductase family. *Proc. Natl. Acad. Sci. USA* **89**, 5015–5019.
14. Ermler, U., Siddiqui, R.A., Cramm, R. & Friedrich, B. (1995). Crystal structure of the flavohemoglobin from *Alcaligenes eutrophus* at 1.75 Å resolution. *EMBO J.* **14**, 6067–6077.
15. Bruns, C.M. & Karplus, P.A. (1995). Refined crystal structure of spinach ferredoxin reductase at 1.7 Å resolution: oxidized, reduced and 2′-phospho-5′-AMP bound states. *J. Mol. Biol.* **247**, 125–145.
16. Correll, C.C., Batie, C.J., Ballou, D.P. & Ludwig, M.L. (1992). Phtalate dioxygenase reductase: a modular structure for electron transfer from pyridine nucleotides to [2Fe–2S]. *Science* **258**, 1604–1610.
17. Lu, G., Campbell, W.H., Schenider, G. & Lindqvist, Y. (1994). Crystal structure of the FAD-containing fragment of corn nitrate reductase at 2.5 Å resolution: relationship to other flavoprotein reductases. *Structure* **2**, 809–821.
18. Nishida, H., Inaka, K., Yamanaka, M., Kaida, S., Kobayashi, K. & Miki, K. (1995). Crystal structure of NADH-cytochrome b_5 reductase from pig liver at 2.4 Å resolution. *Biochemistry* **34**, 2763–2767.
19. Gilles-Gonzales, M.A., Gonzales, G. & Perutz, M.F. (1995). Kinase activity of oxygen sensor FixL depends on the spin state of its heme iron. *Biochemistry* **34**, 232–236.
20. Wakabayashi, S., Matsubara, H. & Webster, D.A. (1986). Primary sequence of a dimeric bacterial haemoglobin from *Vitreoscilla*. *Nature* **322**, 481–483.
21. Tsai, P.S., Hatzimanikatis, V. & Bailey, J.E. (1995). Effect of *Vitreoscilla* hemoglobin dosage on microaerobic *Escherichia coli* carbon and energy metabolism. *Biotechnol. Bioeng.* **49**, 139–150.
22. Tsai, P.S., Nägeli, M. & Bailey, J.E. (1995). Intracellular expression of *Vitreoscilla* hemoglobin modifies microaerobic *Escherichia coli* metabolism through elevated concentration and specific activity of cytochrome *o. Biotechnol. Bioeng.* **49**, 151–160.
23. Dikshit, R.P., Dikshit, K.L., Liu, Y. & Webster, D.A. (1992). The bacterial hemoglobin from *Vitreoscilla* can support the aerobic growth of *Escherichia coli* lacking terminal oxidases. *Arch. Biochem. Biophys.* **293**, 241–245.
24. Liu, C.Y. & Webster, D.A. (1974). Spectral characteristics and interconversions of the reduced, oxidized, and oxygenated forms of purified cytocrome *o. J. Biol. Chem.* **249**, 4261–4266.
25. Webster, D.A. & Orii, Y. (1977). Oxygenated cytochrome *o. J. Biol. Chem.* **252**, 1834–1836.
26. Tyree, B. & Webster, D.A. (1978). The binding of cyanide and carbon monoxide to cytocrome o purified from *Vitreoscilla. J. Biol. Chem.* **253**, 6988–6991.
27. Orii, Y. & Webster, D.A. (1986). Photodissociation of oxygenated cytochrome *o*(s) (*Vitreoscilla*) and kinetic studies of reassociation. *J. Biol. Chem.* **261**, 3544–3547.
28. Khosla, C. & Bailey, J.E. (1989). Evidence of partial export of *Vitreoscilla* hemoglobin into the periplasmic space in *Escherichia coli*: implication for protein function. *J. Mol. Biol.* **210**, 79–89.
29. Khosravi, M., Webster, D.A. & Stark, B.C. (1990). Presence of the bacterial hemoglobin gene improves a-amylase production of a recombinant *Escherichia coli* strain. *Plasmid* **24**, 190–194.
30. Magnolo, S.K., *et al.*, & Hughes, D.E. (1991). Actinorhodin production by *Streptomyces coelicor* and growth of *Streptomyces lividans* are improved by the expression of a bacterial hemoglobin. *Bio/Technol.* **9**, 473–476.
31. Takano, T. (1977). Structure of myoglobin refined at 2.0 Å resolution: crystallographic refinement of metmyoglobin from sperm whale. *J. Mol. Biol.* **110**, 537–568.
32. Ptitsyn, O.B. (1974). Invariant features of globin primary structure and coding of their secondary structure. *J. Mol. Biol.* **88**, 287–300.
33. Bolognesi, M., Onesti, S., Gatti, G., Coda, A., Ascenzi, P. & Brunori, M. (1989). *Aplysia limacina* myoglobin: crystallographic analysis at 1.6 Å resolution. *J. Mol. Biol.* **205**, 529–544.
34. Perutz, M.F. (1993). The role of aromatic rings as hydrogen-bond acceptors in molecular recognition. *Phil. Trans. R. Soc. A* **345**, 105–112.
35. Honzatko, R.B., Hendrickson, W.A. & Love, W.E. (1985). Refinement of a molecular model for lamprey hemoglobin from *Petromyzon marinus. J. Mol. Biol.* **184**, 147–164.
36. Perutz, M.F. (1989). Mechanisms of cooperativity and allosteric regulation in proteins. *Q. Rev. Biophys.* **22**, 139–236.
37. Gonzales-Prevatt, V. & Webster, D.A. (1980). Purification and properties of NADH-cytochrome *o* reductase from *Vitreoscilla. J. Biol. Chem.* **255**, 1478–1482.
38. Kanak, L., Dikshit, L., Spaulding, D., Braun, A. & Webster, D.A. (1989). Oxygen inhibition of globin gene transcription and bacterial haemoglobin synthesis in *Vitreoscilla. J. Gen. Microbiol.* **135**, 2601–2609.

39. Jakob, W., Webster, D.A. & Kroneck, P.M. (1992). NADH-dependent methemoglobin reductase from the obligate aerobe *Vitreoscilla*: improved method of purification and reexamination of prosthetic groups. *Arch. Biochem. Biophys.* 292, 29–33.
40. Bisig, D.A., Di Iorio, E.E., Diederichs, K., Winterhalter, K.H. & Piontek, K. (1995). Crystal structure of Asian elephant *(Elephas maximus)* cyano-metmyoglobin at 1.78 Å resolution. Phe29(B10) accounts for its unusual ligand binding properties. *J. Biol. Chem.* 270, 20754–20762.
41. Quillin, M.L., Arduini, R.M., Olson, J.S. & Phillips, G.N., Jr. (1993). High-resolution crystal structures of distal histidine mutants of sperm whale myoglobin. *J. Mol. Biol.* 234, 140–155.
42. Rizzi, M., Wittenberg, J.B., Coda, A., Ascenzi, P. & Bolognesi, M. (1996). Structural bases for sulfide recognition in *Lucina pectinata* hemoglobin I. *J. Mol. Biol.* 258, 1–5.
43. De Baere, I., Perutz, M.F., Kiger, L., Marden, M.C. & Poyart, C. (1994). Formation of two hydrogen bonds from the globin to the heme-linked oxygen molecule in *Ascaris* hemoglobin. *Proc. Natl. Acad. Sci. USA* 91, 1594–1597.
44. Yang, J., Klock, A.P., Goldberg, D.E. & Mathews, F.S. (1995). The structure of *Ascaris* hemoglobin domain I at 2.2 Å resolution: molecular features of oxygen avidity. *Proc. Natl. Acad. Sci. USA* 92, 4224–4228.
45. Carver, T.E., *et al.,* & Olson, J.S. (1992). A novel site-directed mutant of myoglobin with unusually high affinity and low autooxidation rate. *J. Biol. Chem.* 267, 14443–14450.
46. Springer, B.A., Sligar, S.G., Olson, J.S. & Phillips, G.N., Jr. (1994). Mechanisms of ligand recognition in myoglobin. *Chem. Rev.* 94, 699–714.
47. Travaglini-Allocatelli, C., Cutruzzolà, F., Brancaccio, A., Vallone, B. & Brunori, M. (1994). Engineering *Ascaris* hemoglobin affinity in sperm whale myoglobin; role of tyrosine B10. *FEBS Lett.* 352, 63–66.
48. Stryer, L., Kendrew, J.C. & Watson, H.C. (1964). The mode of attachment of the azide ion to sperm whale met myoglobin. *J. Mol. Biol.* 8, 96–104.
49. Rizzi, M., Ascenzi, P., Coda, A., Brunori, M. & Bolognesi, M. (1993). Molecular bases for heme : ligand recognition in sperm whale *(Physeter catodon)* and *Aplysia limacina* myoglobin. *Rend. Fis. Acc. Lincei, s.9,* 4, 65–73.
50. Conti, E., *et al.,* & Bolognesi, M. (1993). X-ray crystal structure of ferric *Aplysia limacina* myoglobin in different liganded states. *J. Mol. Biol.* 233, 498–508.
51. Janin, J. & Chothia, C. (1990). The structure of protein–protein recognition sites. *J. Biol. Chem.* 265, 16027–16030.
52. Royer, W.E., Jr. (1994). High resolution crystallographic analysis of a co-operative dimeric hemoglobin *J. Mol. Biol.* 235, 657–681.
53. Mitchell, D.T., Kitto, G.B. & Hackert, M.L. (1995). Structural analysis of monomeric hemichrome and dimeric cyanomet hemoglobins from *Caudina arenicola. J. Mol. Biol.* 251, 421–431.
54. Kolatkar, P.R., Hackert, M.L. & Riggs, A.F. (1994). Structural analysis of *Urechis caupo* hemoglobin. *J. Mol. Biol.* 237, 87–97.
55. Brancaccio, A., *et al.,* & Olson, J. (1994). Structural factors governing azide and cyanide binding to mammalian metmyoglobins. *J. Biol. Chem.* 269, 13843–13853.
56. Tarricone, C., Calogero, S., Galizzi, A., Coda, A., Ascenzi, P. & Bolognesi, M. (1997). Expression, purification, crystallization and preliminary X-ray diffraction analysis of the homodimeric bacterial hemoglobin from *Vitreoscilla stercoraria. Proteins* 27, 154–156.
57. Leslie, A.G.W. (1992). *Joint CCP4 and ESF-EACBM Newsletter on Protein Crystallography, No. 26*. Daresbury Laboratory, Warrington, UK.
58. CCP4. (1994). The collaborative computational project number 4 suite: programs for protein crystallography. *Acta Cryst. D* 50, 760–767.
59. Bernstein, F.C., *et al.,* & Tasumi, M. (1977). The protein data bank: a computer-based archival file for macromolecular structures. *J. Mol. Biol.* 112, 535–542.
60. Sheldrick, G.M. (1990). Heavy atom location using SHELXS-90. *Proceedings of the CCP4 Study Weekend: Isomorphous Replacement and Anomalous Scattering*. pp. 23–38, SERC Daresbury Laboratory, Warrington, UK.
61. Abrahams, J.P. & Leslie, A.G.W. (1996). Methods used in the structure determination of bovine mitochondrial F_1 ATPase. *Acta Cryst.* D 52, 30–42.
62. Brünger, A.T. (1992). *X-PLOR, Version 3.1: A System for X-ray Crystallography and NMR*. Yale University Press, New Haven, CT, USA.
63. Tong, L. & Rossmann, M.G. (1990). The locked rotation function. *Acta Cryst. A* 46, 783–792.
64. Read, R.J. (1986). Improved Fourier coefficients for maps using phases from partial structures with errors. *Acta Cryst.* A 42, 140–149.
65. Jones, T.A., Zou, J.Y., Cowan, S.W. & Kjeldgaard, M. (1991). Improved methods for building protein models in electron-density maps and the location of errors in these models. *Acta Cryst.* A 47, 110–119.
66. Tronrud, D.E., Ten Eyck, L.F. & Matthews, B.W. (1987). An efficient general-purpose least-squares refinement program for macromolecular structures. *Acta Cryst. A* 43, 489–501.
67. Laskowski, R.A., Arthur, M.W.M., Moss, D.S. & Thornton, J.M. (1993). PROCHECK: a program to check the stereochemical quality of protein structures. *J. Appl. Cryst.* 26, 283–291.
68. Kraulis, J. (1991). MOLSCRIPT: a program to produce both detailed and schematic plots of protein structures. *J. Appl. Cryst.* 24, 946–950.
69. Higgins, D.G., Bleasby, A.S. & Fuchs, R. (1991). CLUSTALV: improved software for multiple sequence alignment. *CABIOS* 5, 151–153.